Paper 30

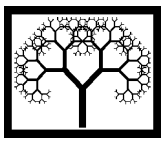

Proceedings of the Fourth International Conference
on Engineering Computational Technology,
B.H.V. Topping and C.A. Mota Soares (Editors),
Civil-Comp Press, Stirling, Scotland.

Identification of a 3D Shape from a 2D Design: Application to a Swimming Monofin

M.A. Luersen†‡, R. Le Riche* and D. Lemosse†
†LMR - Laboratoire de Mécanique, INSA de Rouen, France
‡Mechanical Engineering Department, CEFET-PR, Curitiba, Brazil
***CNRS UMR 5146 / SMS, Ecole des Mines de Saint Etienne, France**

Abstract

The models of 3D unsteady coupled fluid-structure systems such as swimming fins are numerically too expensive to be optimized. Designers must therefore make preliminary decisions based on simplified models. In particular, considering 2D cases for optimization is a standard practice. The 2D design then needs to be translated into its 3D counterpart.

This work is an example of such a problematics. The objective is to design a 3D swimming monofin using a 2D optimal flexural stiffness distribution determined in [1]. For marketing and manufacturing cost reasons, the fin planform shape is given. The 2D flexural stiffnesses are therefore mapped into a 3D fin thickness distribution. The 3D thickness distribution is found by minimizing a distance between the 2D and 3D models which expresses a static, modal or a mix of static and modal equivalence. The effects of the identification formulations on the final thickness distribution are studied.

Keywords: monofin design, swimming propulsion, identification, optimization.

1 Introduction

Although monofins already provide the most efficient way of swimming for human beings, it is expected that further progress can be achieved because today's monofin design is empirical and studies in aquatic locomotion modes and oscillating hydrofoils show that more efficient swimming systems exist. Fish like tuna, mackerel, sharks and marine mammals have propulsive efficiency greater than 90% at high swimming speed in calm waters ([2]). Similar efficiencies have been observed for artificial oscillating hydrofoils ([3, 4]). Previous works have been devoted to describing the physics and physiology of fin-swimming ([5], [6]).

The 3D models available for unsteady coupled fluid-structure systems are numerically too expensive to be used in an optimization process. Designers must therefore make preliminary decisions based on simplified models. In particular, considering 2D cases for optimization is a standard practice. The 2D design then needs to be translated into its 3D counterpart.

The objective of the current work is to design a 3D swimming monofin using the 2D optimal flexural stiffness distribution determined in [1]. In this study, a 2D monofin was represented by rigid bars linked by torsional springs, in dynamic equilibrium with the fluid. The swimmer was composed of linear articulated segments, whose kinematics was imposed and identified from experimental data. The sheet vortex fluid model presented in [7] was used, which accounts for a two-dimensional unsteady, inviscid and incompressible fluid flow going past a thin obstacle. Because of its low memory and time consumption, this is considered as one of the most accurate models that can be optimized. The propulsive power provided by the monofin has been maximized with an upper bound on the total power expended by the swimmer. The design variables were the spring rigidities and the optimization problem was solved by the Globalized and Bounded Nelder-Mead (GBNM) algorithm ([8]). On a standard PC, the optimization took about $56\ h$.

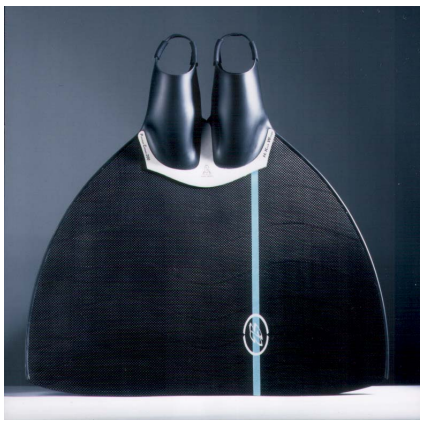

Figure 1: Carbon monofin (Breier©).

The flexural stiffness distribution obtained from the two-dimensional optimization is now translated into a three-dimensional shape. The mapping can be seen as an identification procedure where the "experience" is a 2D bars system whose behavior is approximated by a 3D finite element model of the fin. In its most general statement, this identification problem is ill-posed since many combinations of shape and thickness distribution can represent the 2D monofin. In practice, however, the planform shape of the monofin is dictated by manufacturing (mold cost) and marketing considerations which yield forms that mimick marine mammals. Since the fin planform shape is given, the spring stiffnesses are mapped into the fin thickness distribution. The equivalence between the two models can be sought in terms of static behavior, dynamic behavior, or a mix of static and dynamic behaviors. The advantages of static

equivalence is that the load cases can be taken from the 2D flow simulation and large displacements analyses are available. However, it neglects the fin inertia, which may be realistic in comparison to water inertia and fin flexural stiffness. On the contrary, the modal dynamic identification accounts for both flexural and inertial terms but it is, in essence, a small displacements analysis. The 3D thickness distribution is found by minimizing an error function between the static and/or modal reponse of the 2D and 3D monofins. The GBNM minimization algorithm carries out the identifications.

The rest of the paper is structured as follows. The 2D model and the stiffness monofin optimization is summarized in Section 2. Section 3 describes the mapping from the simplified 2D to the 3D model and the identification problem formulation. The effects of the identification formulations and of the large or small displacements fin models on the final thickness distributions are discussed in Section 4. An appendix analyses flexural identifiability of the 2D system.

2 Monofin Stiffness Optimization

2.1 2D Model

The 2D stiffness optimization problem formulated and solved in [8] is briefly described here. The Reynolds number for the swimmer-fin system is of the order of 10^6, so the viscosity is neglected. By further neglecting obstacles thickness, flow separation and water compressibility, the unsteady vortex based flow model of [7] can be used: the velocity field is obtained by the superposition of a uniform fluid flow and a field induced by vortices emitted at the fins trailing edge. The vortex intensities are calculated at each instant so that the following hold: (i) the flow remains attached along the obstacle; (ii) the flows from the upper and the lower surfaces join smoothly at the trailing edge (Kutta condition); (iii) the total circulation is conserved. The advantage is that only the solid boundary and the wake are discretized, as opposed to meshing the whole domain, so that computer time is saved.

The swimmer is represented by 4 segments: the arms, the torso, the thighs and the tibias. The monofin is modelled by 6 rigid bars articulated by torsional springs with large rotations allowed (Figure 2). All bars have equal and constant linear mass density. From the analysis of a monofin swimmer video the swimmer movement is approximately segment-wise harmonic:

$$y_1(t) \;=\; Y_1^c + Y_1 \sin(2\pi f t)\;, \tag{1}$$

$$\theta_i(t) \;=\; \Theta_i^c + \Theta_i \sin(2\pi f t - \phi_i)\;, \tag{2}$$

where y_1 is the vertical displacement of the hand, θ_1 is the slope between the horizontal and the arms, ϕ_1 is the phase angle between the vertical hand movement and the arm rotation, θ_i ϕ_i, $i = 2, 5$ are the angles and the phases between the segments $(i-1)$ and i, respectively. The parameters of Equations (1) and (2) (the amplitudes Y_1 and Θ_i, the mean values Y_1^c and Θ_i^c, the phase angles ϕ_i and the frequency f) and the

mean swimmer speed (considered to be the free-stream speed) U_∞ are identified from measured vertical displacements of the hand, neck, shoulder, elbow, hip, knee, ankle and toe of a sprint swimmer. The following values are obtained ([9]): $U_\infty = 3.0\,m/s$, $Y_1 = 0.07\,m$, $Y_1^c = 0.0\,m$, $\Theta_1 = 3.4°$, $\Theta_1^c = -1.6°$, $\phi_1 = -222.6°$, $\Theta_2 = 12.0°$, $\Theta_2^c = 1.6°$, $\phi_2 = -152.8°$, $\Theta_3 = 20.0°$, $\Theta_3^c = -10°$, $\phi_3 = 17.2°$, $\Theta_4 = 14.0°$, $\Theta_4^c = 14.0°$, $\phi_4 = 17.2°$, $\Theta_5 = 16.0°$, $\Theta_5^c = -20.0°$ and $\phi_5 = 107.2°$.

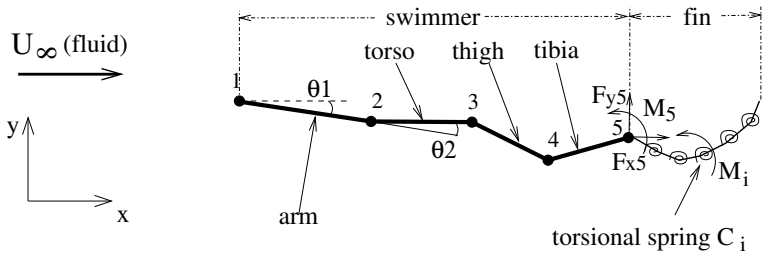

Figure 2: Swimmer and monofin representation.

The displacements of the first monofin bar ($\theta_5(t)$, $x_5(t)$ and $y_5(t)$) are imposed because they follow the feet. The forces distributed over the fin are obtained by means of a coupled fluid-structure calculation. The unknowns of the problem are the orientations, the angular velocities and the angular accelerations of the monofin's bar joints ($\theta_i(t)$, $\dot{\theta}_i(t)$, $\ddot{\theta}_i(t)$, $i = 6, 10$), and the efforts at the point 5 ($F_{x5}(t)$, $F_{y5}(t)$, $M_5(t)$). The monofin dynamic equilibrium equations are solved by the Newmark time integration scheme [10]. At each iteration, the system of non-linear equations is solved using a mixed Newton-Raphson/GBNM scheme. The GBNM algorithm is employed to minimize the residue of the equations when the Newton-Raphson iterations are fruitless. A visualization of the flow, swimmer and monofin is given in Figure 3.

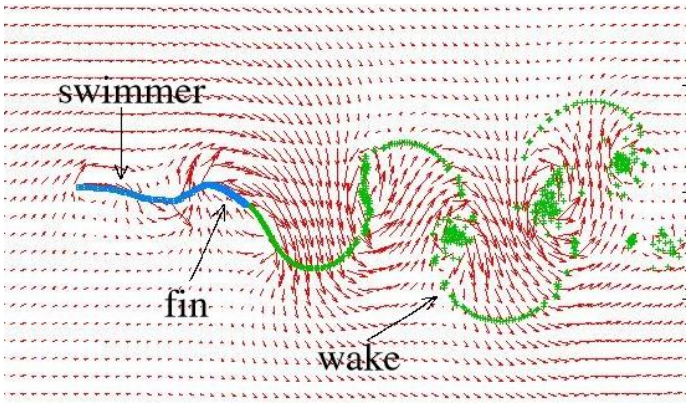

Figure 3: Flow, swimmer and monofin visualization. Continuous trace, the obstacle; $\times$, the wake particles; $\rightarrow$, the relative velocity of the fluid.

2.2 Optimization Problem Formulation

As the majority of the thrust is produced by the monofin, the purpose of the optimization is to maximize the propulsive power provided by the monofin with a constraint on the maximum total power expended by the swimmer at the fin. The time-averaged propulsive power is defined as,

$$\bar{P}_{fx} \;=\; \frac{1}{T_f - T_s} \int_{T_s}^{T_f} \int_{0}^{L_s} f_x(s) |U_\infty| \; ds \; dt \; , \tag{3}$$

and the time-averaged power supplied by the fluid to the fin is,

$$\bar{P}_{f} \;=\; \frac{1}{T_f - T_s} \int_{T_s}^{T_f} \int_{0}^{L_s} (f_x(s)(\dot{x}(s) + |U_\infty|) + f_y(s)\dot{y}(s)) \; ds \; dt \; , \tag{4}$$

where U_∞ is the swimmer's mean forward speed, $\dot{x}$ and $\dot{y}$ are the velocity components of the fin in a stationary reference system with respect to the fluid speed U_∞, $f_x(s)$ and $f_y(s)$ are the fluid forces per unit length over the fin at the fin coordinates, L_s is the monofin's length, T_s and T_f are the starting and final calculation times. Energy transmissions on the swimmers body are neglected in comparison with the fin, consequently $\bar{P}_f$ is considered to be the power provided to the swimmer. From the reference system that has been chosen (see Figure 2), for a swimmer going up-stream, $\bar{P}_{fx}$ and $\bar{P}_f$, calculated by Equations (3) and (4), are negative. Thus, the objective function to be minimized is $\bar{P}_{fx}$ with a lower bound on the total power $\bar{P}_f$. The design variables are the torsional stiffnesses C_i. The optimization problem is formulated as,

$$\begin{cases} \min\limits_{C_i} \bar{P}_{fx} \; , \\ \text{such that,} \\ \bar{P}^{min} \;\leq\; \bar{P}_f \; , \\ C_i^{min} \;\leq\; C_i \;\leq\; C_i^{max} \; , \quad i = 1, 5 \; . \end{cases} \tag{5}$$

2.3 Stiffness Optimization Results

The optimization problem (5) is solved by means of the Globalized and Bounded Nelder-Mead algorithm ([8]). The GBNM is a global optimization method based on probabilistic restart. Local searches are performed by an improved Nelder-Mead algorithm ([11]) where design variables can be bounded, inequality constraints taken into account by adaptive penalization, and some search failure cases prevented. The GBNM does not need gradient calculation.

The optimization problem is solved for the swimmer's total power $\bar{P}^{min} = -2000\, W$. As a comparison, the power mesured on average distance swimmers in [12] was about $1400\, W$. Higher limit accounts for the shorter distance covered by a sprint swimmer and the 2D model that overestimates efforts (the fluid cannot go around the obstacle by the sides and there is no flow separation). Figure 4 shows the optimal stiffness distribution. The stiffnesses are tapered from the leading to the trailing edge.

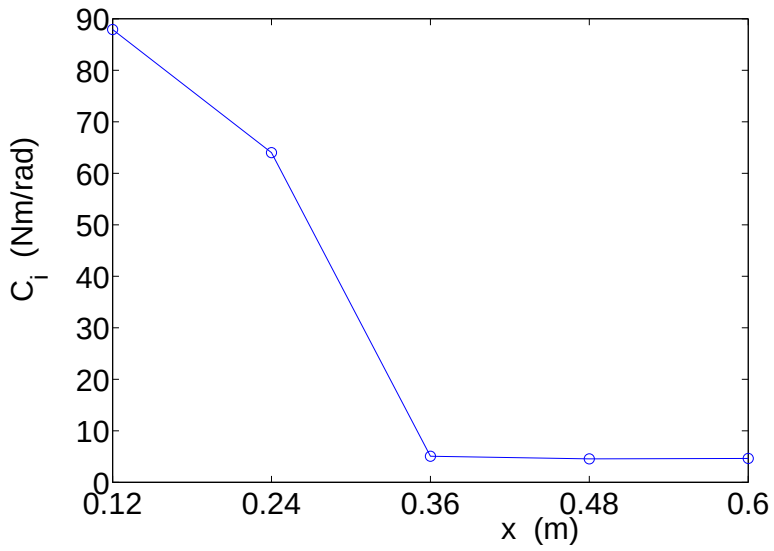

Figure 4: Optimal 2D stiffness distribution.

3 Translation into a 3D Shape

The stiffness distribution obtained from the two-dimensional optimization previously described is now translated into a three-dimensional shape. The mapping can be seen as an identification procedure where the "experience" is a 2D bars system whose behavior is approximated by a 3D finite element model of the fin. In its most general statement, this identification problem is ill-posed since the 3D system has more degrees of freedom than its 2D counterpart. Many combinations of shape and thickness distribution can represent the 2D monofin. In practice, however, the planform shape of the monofin is dictated by manufacturing (cost of molds) and marketing considerations which has yielded forms that mimick marine mammals. Once the fin planform shape is given, the spring stiffnesses can be mapped into a fin thickness distribution. Because the fin is manufactured using composite prepreg layup, the thickness is kept constant spanwise and varies chordwise at ply drops. The equivalence between the two models can be sought in terms of static behavior, modal behavior, or a mix of static and modal behaviors. The advantages of the static equivalence is that large displacements analyses are available ([13]). However, it neglects the fin inertia in comparison to water inertia and fin flexural stiffness. On the contrary, the modal dynamic identification accounts for both fin inertia and flexural stiffness but it is, in essence, a small displacements analysis. Furthermore, 3D non-bending modes have no pendant in the 2D system. For this reason, only the first natural mode, which has empirically been found on the monofin to consistently be bending, is considered. The 3D thickness distribution is found by minimizing

$$J = \alpha J_{static} + (1 - \alpha) J_{freq} \, , \tag{6}$$

where,

$$J_{static} = \sum_{i=1}^{NCP} \frac{((u_i - \tilde{u}_i)^2 + (v_i - \tilde{v}_i)^2)}{(u_i^2 + v_i^2)} \quad \text{and} \quad J_{freq} = \frac{|w_1^2 - \tilde{w}_1^2|}{w_1^2} \, . \tag{7}$$

α is a weight factor between static displacement and modal criteria, (u_i, v_i) are the target displacements at the bar joints of the simplified model, $(\tilde{u}_i, \tilde{v}_i)$ are the displacements at the NCP corresponding control points of the finite element model, w_1 is the target first natural circular frequency of the simplified model and $\tilde{w}_1$ is the first natural circular frequency of the finite element model.

The 3D fin is analyzed with a finite element model which relies on solid elements improved for thin structures ([13]). The parameterization of the fin is described in Figure 5.

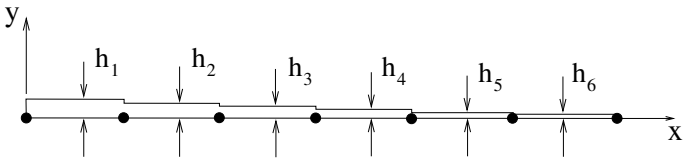

(a)

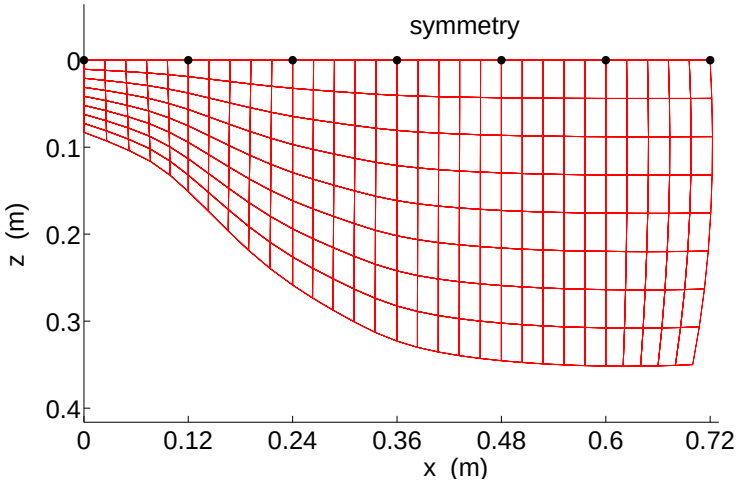

(b)

Figure 5: Fin parameterization: thickness profile (a), half-planform shape and finite element mesh (b). The dots represent the points where J_{static} is evaluated.

The final thickness distribution is identified by solving,

$$\begin{cases} \min\limits_{h_i} J \ , \\ \text{such that,} \\ h_i^{min} \ \leq \ h_i \ \leq \ h_i^{max} \ , \quad i = 1,6 \ and \\ h_i \ \leq \ h_{i-1} \ , \quad i = 2,6 \end{cases} \tag{8}$$

where the thicknesses h_i are bounded by $h_i^{min} = 1.5 \times 10^{-4}\, m$ and $h_i^{max} = 2 \times 10^{-2}\, m$, $i = 1,6$. The constraints $h_i \ \leq \ h_{i-1}$, $i = 2,6$, are handled by reordering the variables h_i in the finite element (FE) analysis but keeping them unordered in the optimization. It was observed on the current problem that this arrangement is more efficient than the adaptive penalization of the GBNM optimizer.

4 Identification Results and Discussion

Firstly, when $J = J_{static}$ ($\alpha = 1$), the influence of the load cases and the small or large displacements analyses are described. Three different vertical load cases are tested, as sketched in Figure 6. It should be noted that there are two necessary conditions for $h^* = arg\min J_{static}$ to be unique: 1) the equilibrium relative angles should be non-null (see Appendix A); 2) there should be at least as many control points, NCP, as there are design variables (6 here), otherwise many combinations of design variables may produce the same displacements at the control points.

Secondly, the difference between minimizing J_{static} and J_{freq} is exhibited.

Finally, the problem is solved for a mixed static and modal criterion ($\alpha = 0.5$).

The GBNM algorithm is used to solve problem (8). In order to protect the final design found in this work, a material description is intentionally left out and the ply thicknesses are normalized.

4.1 Static Small Displacements Formulation

First, a static analysis procedure ($\alpha = 1$) under small displacements is carried out. The three load cases of Figure 6 are tested setting $p_1 = 4.0875\ N/m$, $F_2 = 0.73575\ N$ and $p_3 = 4.0875\ N/m$. The identified thicknesses obtained for this formulation are presented in Figure 7. For the load cases considered, it can be noted that thickness distributions are very close, the main difference being a 2.5% variation in the h_2 value. Figure 8 shows the deformed positions of the simplified 2D bars model and the mid-plane symmetry line ($z = 0$) of the FE model built using the thicknesses identified under load case 1.

4.2 Static Large Displacements Formulation

The three load distributions used in the small displacements identification are kept but the intensities are six times higher in order to generate a large displacements problem:

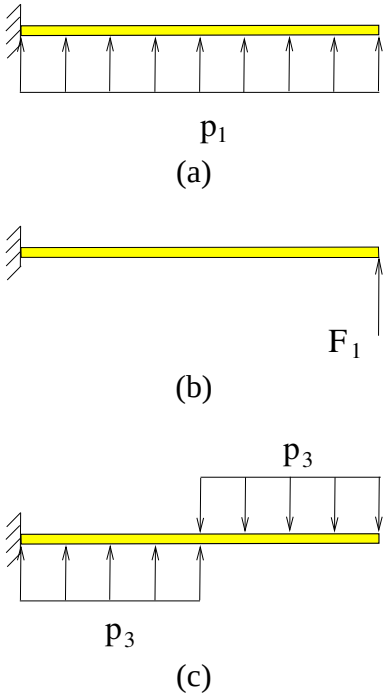

Figure 6: The load cases considered for the thickness identification.

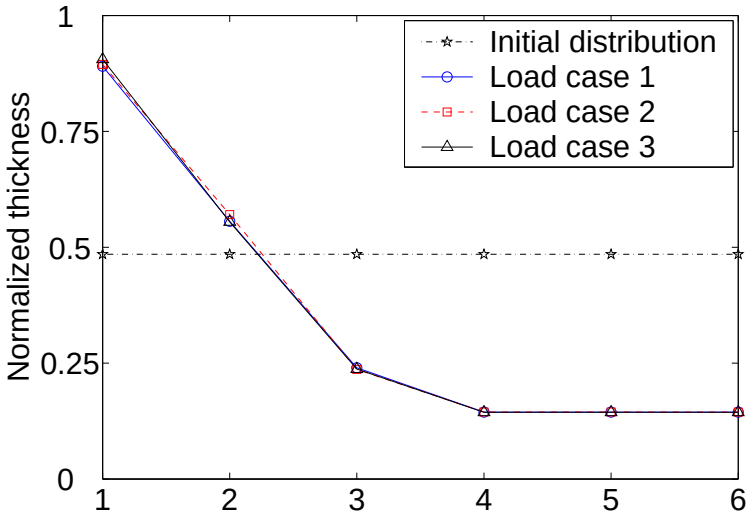

Figure 7: Normalized identified thickness distributions for small displacements formulation.

$p_1 = 24.525\ N/m$, $F_2 = 4.4145\ N$ and $p_3 = 24.525\ N/m$.

The identified thicknesses are presented in Figure 9. For the load cases considered,

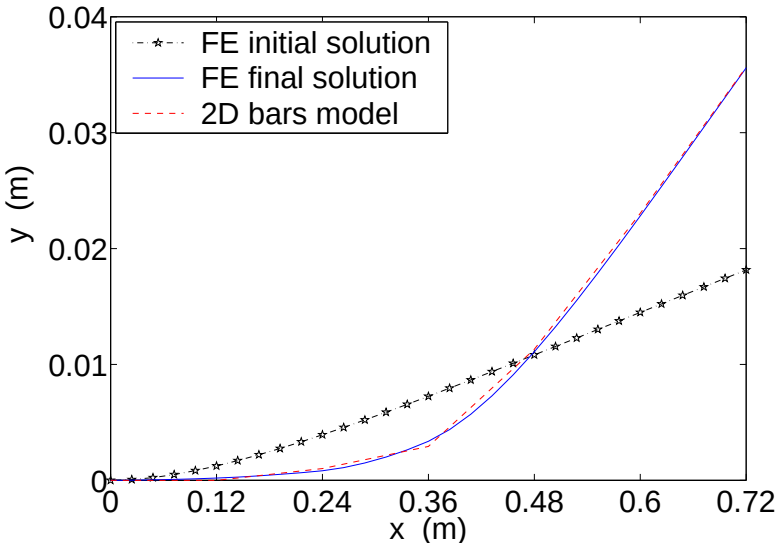

Figure 8: Deformed shapes comparison for small displacements formulation, load case 1.

it can be noted that thickness distributions are close, the main difference being a 9% variation in the h_2 value. Figure 10 shows the deformed shape of the bars model and the mid-plane symmetry line ($z = 0$) of the FE model built using the identified thicknesses under load case 1.

Table 1 shows the first natural frequency of the 3D fin for static formulation solutions. The reader should keep in mind that frequencies are not accounted for in the static identifications. The difference in $\tilde{f}_1$ is less than 0.5% and 1.8% among small and large displacements solutions, respectively. For all static formulations it is less than 3.5%.

Load case	Small displacements	Large Displacements
1	2.4842	2.5584
2	2.4777	2.5137
3	2.4720	2.5208

Table 1: First natural frequency ($\tilde{f}_1 = \frac{\tilde{w}_1}{2\pi}$), in hz, for static formulation solutions.

It is observed that for the static small displacements formulation the load case influence is very small. For the large displacements procedure there is a higher difference among the results obtained with different load cases, probably because in a large displacements analysis the displacements are stress dependent. The solutions in small and large displacements are close, with large displacements solutions being thicker near the monofin's leading edge (see Figure 12). This is explained by the fact that

large displacements analysis generates larger vertical displacements in the clamped region.

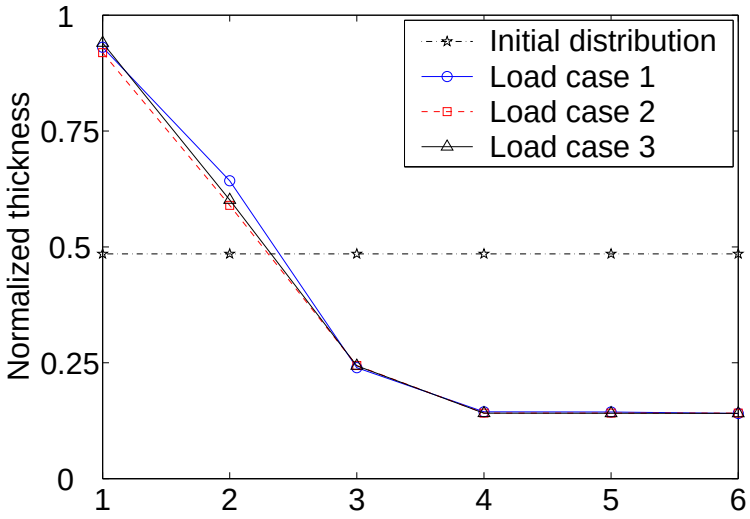

Figure 9: Normalized identified thickness distributions for large displacements formulation.

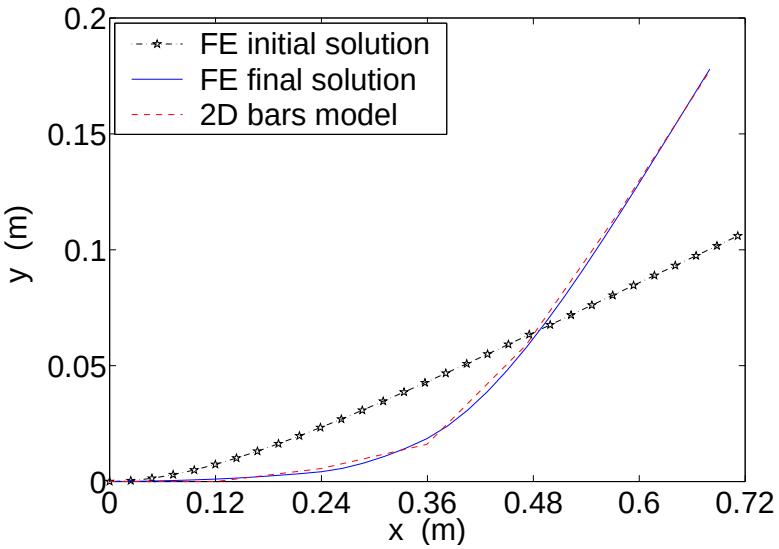

Figure 10: Deformed shapes comparison for large displacements formulation, load case 1.

4.3 First Natural Frequency Formulation

In this identification procedure, only the first natural frequency is considered ($\alpha = 0$). The first natural frequency of the 2D system is $f_1 = \frac{w_1}{2\pi} = 1.5400\ hz$. It was numerically observed that this formulation presents many solutions that are very close, i.e., many thickness distributions correspond to the frequency f_1. Figure 11 shows the solutions found by the GBNM optimization algorithm having a deviation smaller than $1 \times 10^{-4}\ hz$, and the corresponding modes. Note that the GBNM algorithm has a restart procedure which permits to locate different local optima in a single run.

There are several solutions going from highly tapered to uniform thickness. The maximum amplitude is at trailing edge for all solutions. The maximum curvature changes, moving from the clamped region for Solution 1, towards the trailing edge for Solutions 2 and 3, respectively.

4.4 Mixed Formulation

In order to take into account both static and dynamic behaviors of the monofin, a mixed criterion ($\alpha = 0.5$) is used. For the static analysis, only load case 1 under small displacements is considered since load cases do not generate different solutions (at the condition that the equilibrium angles are non-null, cf. Appendix A), and the discrepancies between large and small displacements solutions are negligible.

Figure 12 compares solutions to the mixed, the static linear (small displacements and $\alpha = 1$), and the static non-linear (large displacements and $\alpha = 1$) problems. Figure 13 shows the deformed shapes of the bars model and the mid-plane symmetry line ($z = 0$) of the FE model built with the identified thicknesses. For the mixed formulation solution, the first natural frequency of the finite element model is $\tilde{f}_1 = \frac{\tilde{w}_1}{2\pi} = 2.2115\ hz$.

In comparison to the static analysis formulations, material is removed from the clamped region and added at the tip. This provides lower first natural frequency, which is closer to the 2D model. This is traded against a slight departure from the targetted static deformed shape.

5 Conclusions

It is common that the most accurate 3D models of a system are numerically too expensive for design. In such cases the optimization is performed on a simplified 2D model. The solution has then to be translated into the realistic 3D expression.

The design of a swimming monofin is an illustration of such a general problematics. Analysis of the system requires an instationary coupled fluid-structure calculation.

A strategy for translating the 2D simplified fin model into a 3D fin has been presented. The shape and the material of the monofin are fixed by manufacturing constraints. The thickness distribution is identified to be statically and/or dynamically

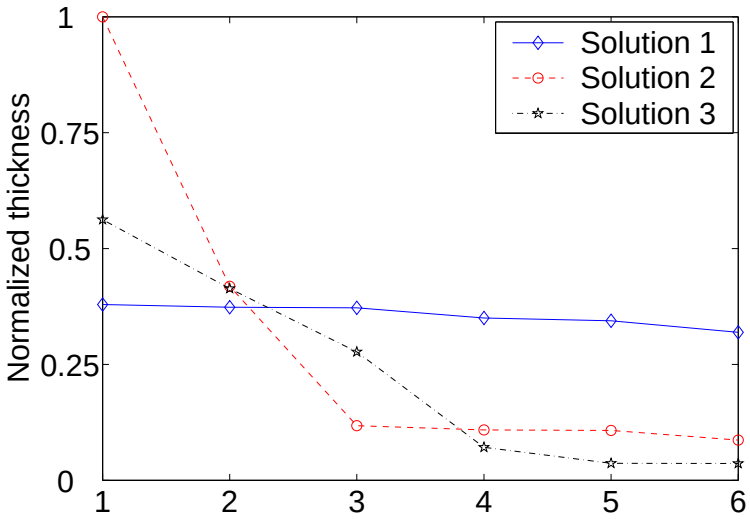

(a)

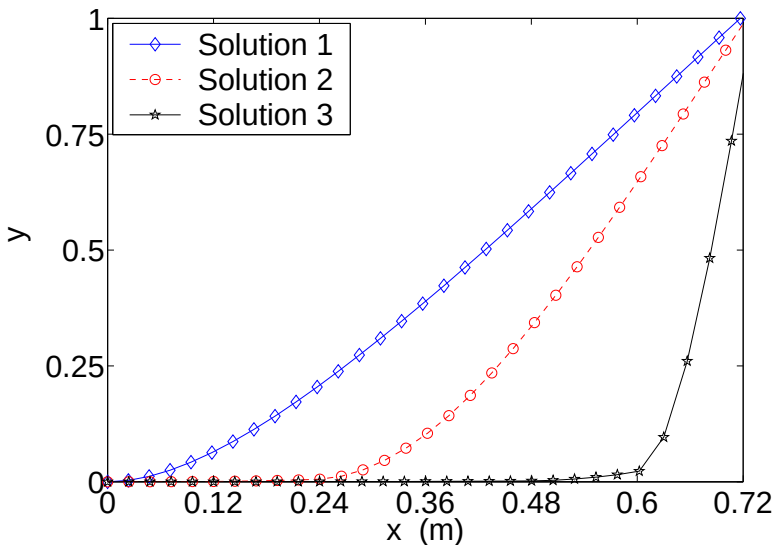

(b)

Figure 11: Normalized identified thickness distributions for first natural frequency formulation (a) and correspondig modes, normalized by the maximal vertical displacement (b).

equivalent to the optimized 2D system. The GBNM algorithm performs the identification. The influence of the various formulations and load cases on the final thickness distributions have been studied.

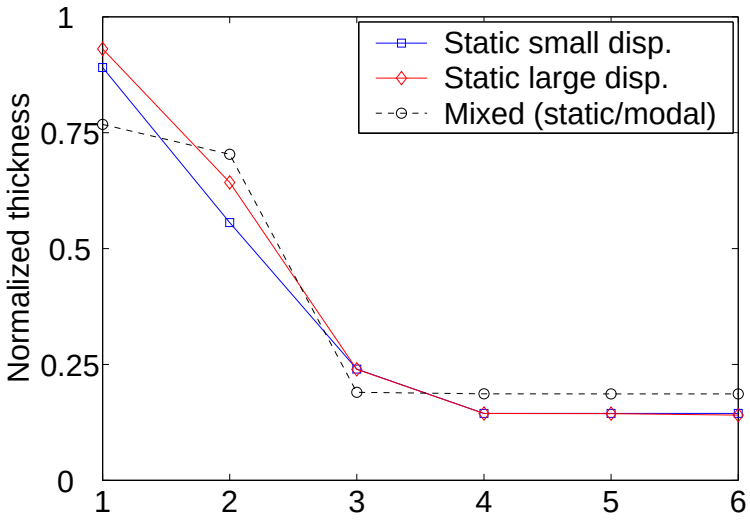

Figure 12: Comparison among the three identification formulations.

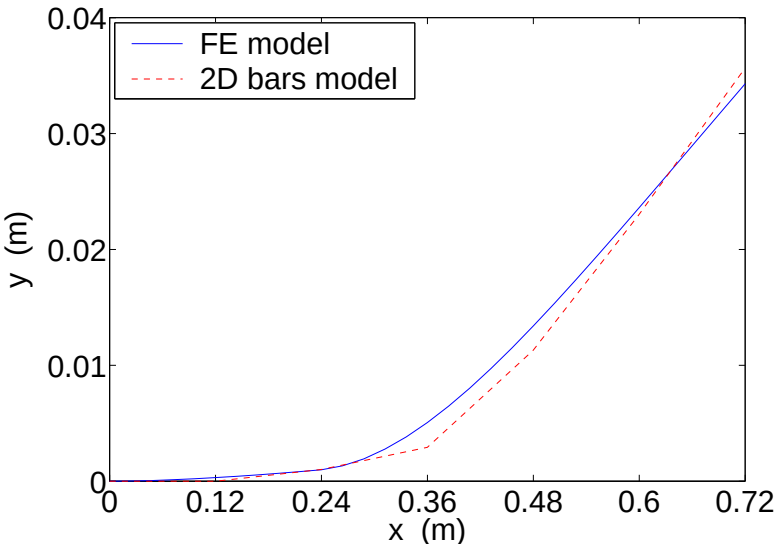

Figure 13: Deformed shapes comparison for mixed formulation, load case 1.

It is recommended to choose the mixed static/dynamic formulation when translating a 2D fin design into 3D. Indeed, the static and dynamic formulations do no yield the same designs. In particular, it was found that the 2D model, which has a constant chordwise mass density, has a dynamic behavior which cannot be reproduced by 3D fins.

In terms of static analysis, a small displacements finite element model is sufficient. It is observed that small and large displacements formulations do not present significant design differences. Moreover, when mixed formulation is considered, a highly accurate static analysis is not essencial because static and dynamic equivalences between the 2D and 3D models are traded-off, so that there is no longer a precise deformed shapes match.

6 Acknowledgements

Fundings for this work were provided by CNPq Brazilian research agency for the first author and by the Breier fin company, France.

References

[1] M.A. Luersen, R. Le Riche, D. Lemosse, O. Le Maître, *"Swimming Monofin Optimization"*. Submited to the 10th AIAA/ISSMO Multidisciplinary Analysis and Optimization Conference, Albany, New York, Aug. 30 - Sept. 1, 2004.

[2] M. Sfakiotakis, D.M. Lane, B.C. Davies, *"Review of Fish Swimming Modes for Aquatic Locomotion"*, IEEE J. of Oceanic Eng., 24(2), 237-252, 1999.

[3] G. Pedro, A. Suleman, N. Djilali, *"A numerical study of the propulsive efficiency of a flapping hydrofoil"*, International Journal for Numerical Methods in Fluids, 42, 493-526, 2003.

[4] J.M. Anderson, K. Streitlien, D.S. Barret, M.S. Triantafyllou, *"Oscillating foils of high propulsive efficiency"*. Journal of Fluids Mechanics, 360, 41-72, 1998.

[5] P. Zamparo, D.R. Pendergast, D.R., B. Termin, A.E. Minetti, *"How fins affect the efficiency and economy of human swimming"*, The International Journal of Experimental Biology, 205, 2665-2676, 2002.

[6] L. Baly, A. Durey, D. Favrier, *"Etude des fréquences et amplitudes ondulatoires chez le nageur avec palmes de haut niveau"*. Journées de l'Ecole Doctorale des Sciences de la Vie et de la Santé, LABM, UMSR 2164, CNRS, Univ. de Méditerranée, France, 2001 (http://www.ujf-grenoble.fr/ufraps/acaps/Actes/Poster/baly.pdf) (in French).

[7] O. Le Maître, S. Huberson, E. Souza de Cursi, *"Unsteady model of sail and flow interaction"*. Journal of Fluids and Structures, 13, 37-59, 1999.

[8] M.A. Luersen, R. Le Riche, F. Guyon, *"A constrained, globalized, and bounded Nelder-Mead method for engineering optimization"*, Structural and Multidisciplinary Optimization, Springer, Vol. 27, 43-54, 2004.

[9] M.A. Luersen, R. Le Riche, O. Le Maître, E. Breier, *"Optimisation de monopalmes de nage"*. Proc. of the 6th Colloque National en Calcul des Structures, Vol. 3, 207-214, CSMA/AFM publ., Giens, France, May 2003, (in French).

[10] M. Géradin, A. Cardona, *"Flexible Multibody Dynamics: A Finite Element Approach"*. John Wiley & Sons, Inc., New York, USA, 2001.

[11] J.A. Nelder, R. Mead, *"A simplex for function minimization"*, Computer J. 7, 308-313, 1965.
[12] P.E. di Prampero, D.R., Pendergast, D.W. Wilson, D.W., Rennie, *"Energetics of swimming in man"*. Journal of Applied Physiology, 360(1), 1-5, 1974.
[13] D. Lemosse, G. Dhatt, *"Study of Shell-like Structures by Brick Finite Element Model"*, Proceedings of The 5th International Conference on Computational Structures Technology, Vol. H, pp. 183-190, Leuven, Belgium, 6-8 Septembre 2000.

A Flexural Stiffness Identifiability

When choosing the load cases under which J_{static} is calculated (Equation (7)), care should be taken to guarantee that the optima are locally unique (local identifiability property). In this regard, it is convenient and sufficiently descriptive to study under which conditions on the loads F_i the 2D bars system of Figure 14 has a unique set of stiffnesses C_i associated to an equilibrium position θ_i^*, $i = 1, n$.

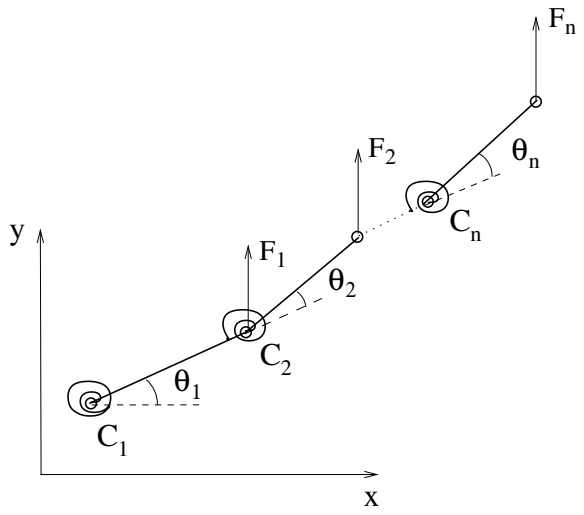

Figure 14: 2D bars system. All bars have lenght l, C_i is the stiffness of the i-th joint, the loads F_i are vertical.

The equilibrium equations of the system are,

$$\begin{cases} C_1\theta_1 = lF_1\cos\theta_1 + lF_2(\cos\theta_1 + \cos(\theta_1+\theta_2)) + \cdots + \\ \qquad + lF_n(\cos\theta_1 + \cdots + \cos(\theta_1+\cdots+\theta_n)) \\ \quad \cdots \\ C_n\theta_n = lF_n\cos(\theta_1+\cdots+\theta_n)\ , \end{cases} \tag{9}$$

or,

$$h_i(\theta_1, \ldots, \theta_n) = 0\ , \quad i = 1, n\ . \tag{10}$$

Let θ_i^*, $i = 1, n$, satisfy the equilibrium equations (10). To see how a change in C_i's affects the equilibrium of the system, a first order approximation to the h_i's is written at θ^*,

$$\left[\frac{\partial h}{\partial C}(\theta^*)\right] \Delta C = 0 \,, \tag{11}$$

where components of the Jacobian matrix are, in general,

$$\left[\frac{\partial h}{\partial C}(\theta^*)\right]_{ij} = \frac{\partial h_i}{\partial C_j}(\theta^*) = \frac{dh_i}{dC_j}(\theta^*) + \sum_{k=1}^{n} \frac{\partial h_i}{\partial \theta_k}(\theta^*) \frac{\partial \theta_k}{\partial C_j}(\theta^*) \,. \tag{12}$$

Cases of interest are the problematic ones where, around θ_i^*, a change in C_i's induces no change in the equilibrium, i.e., cases where there are an infinite number of C_i's associated to the same deflected shape θ^* (same J_{static}). At such non-identifiable points, by definition,

$$\frac{\partial \theta_k}{\partial C_j}(\theta^*) = 0 \tag{13}$$

and the Jacobian has null eigenvalues whose associated eigenvectors (stiffness change ΔC) induce no variation of the equilibrium. When (13) holds,

$$\left[\frac{\partial h}{\partial C}(\theta^*)\right]_{ij} = \frac{\partial h_i}{\partial C_j}(\theta^*) = \theta_i^* \delta_{ij} \,, \tag{14}$$

where $\delta_{ij} = 1$ if $i = j$; $\delta_{ij} = 0$ otherwise.

This establishes that the Jacobian eigenvalues are the equilibrium angles. Local non-identifiability occurs when some of the equilibrium angles are null, which is intuitive since the associated springs have no action. Two typical scenarii where some θ_i^* are null are depicted in Figure 15, first when the tip of the system is not loaded, then when the moments cancel at a joint.

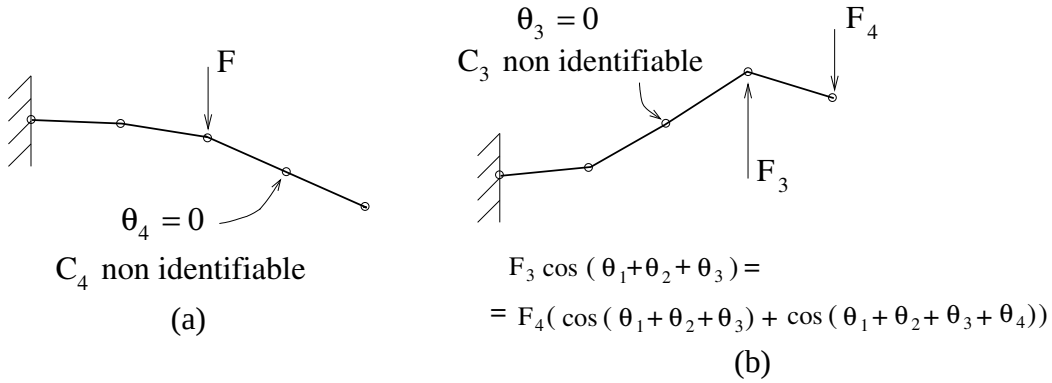

Figure 15: Examples of loads such that the flexural stiffnesses are not identifiable, (a) the tip is not loaded, (b) moments cancel at joint 3.

Besides the load case, we note, without formal proof, that the control points used to calculate J_{static} should be numerous and well spread on the system in order to

guarantee the uniqueness of $\arg\min_{C \text{ or } h} J_{static}$. As a counter-example (see Figure 16), if there is only a control point at the tip with a target displacement (u^t, v^t), it should be clear that there is an infinite number of choices of $(C_1^*, \ldots, C_n^*, \theta_1^*, \ldots, \theta_n^*)$ such that

$$\begin{cases} \text{(10) is satisfied and} \\ l(\cos\theta_1^* + \cdots + \cos(\theta_1^* + \cdots + \theta_n^*)) = u^t \\ l(\sin\theta_1^* + \cdots + \sin(\theta_1^* + \cdots + \theta_n^*)) = v^t \end{cases} \tag{15}$$

because (15) is a system of $(n+2)$ equations in $2n$ unknowns.

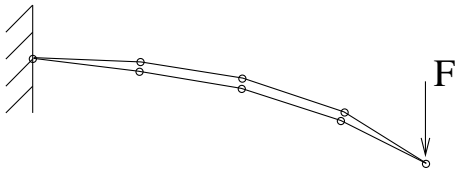

Figure 16: Two deflected shapes that have the same displacements at the tip. This illustrates why C_i's would not be identifiable if there was only a control point at the tip.